Oxygen Kinetics During Corneal Cross-linking With and Without Supplementary Oxygen

THEO G. SEILER, MARIA A. KOMNINOU, MALAVIKA H. NAMBIAR, KASPAR SCHUERCH, BEATRICE E. FRUEH, AND PHILIPPE BÜCHLER

• PURPOSE: To measure and simulate oxygen kinetics during corneal cross-linking at different irradiances with and without supplementary oxygen.
• DESIGN: Experimental, laboratory study.
• METHODS: In de-epithelialized porcine eyes, a femtosecond-laser–generated tunnel was used to place a fiber probe in corneal depths of 100, 200, and 300 μm to measure the local oxygen concentration. After riboflavin imbibition, the corneas were irradiated at 3, 9, 18, and 30 mW/cm^2 while the oxygen concentration was measured. All experiments were performed under normoxic (21%) and hyperoxic (>95%) conditions. The obtained data were used to identify parameters of a numerical model for oxygen consumption and diffusion.
• RESULTS: The equilibrium stromal oxygen concentration under atmospheric oxygen at 3 mW/cm^2 was 2.3% in 100 μm decreasing to <1% in 300 μm. With 9, 18, and 30 mW/cm^2, no oxygen was available in 200 μm, respectively, 100 μm or deeper. Using a hyperoxic environment, the concentration was 50% using 3 mW/cm^2 in 100 μm, decreasing to 40% in 300 μm. At 9 mW/cm^2, the concentrations were 5%, 3%, and 1% in 100, 200 and 300 μm, respectively. Using 18 and 30 mW/cm^2, all oxygen was depleted at 100 μm; however, oxygen half-lives were longer at 18 mW/cm^2 than at 30 mW/cm^2. The oxygen model was able to reproduce the experiments and indicated an exponential decay with increasing distance to the anterior surface.
• CONCLUSION: Supplementary oxygen increases the oxygen availability during corneal cross-linking. At higher irradiances, supplementary oxygen is beneficial and eliminates the bottleneck of oxygen allowing a potentially more efficient cross-linking. The calibrated numerical model can quantify the spatial oxygen concentration related to different scenarios such as irradiance or environmental oxygen concentration. (Am J Ophthalmol 2021;223:368–376. © 2020 The Authors. Published by Elsevier Inc. This is an open access article under the CC BY-NC-ND license (http://creativecommons.org/licenses/by-nc-nd/4.0/).)

Accepted for publication Nov 4, 2020.

From the Klinik für Augenheilkunde, Universitätsklinikum Düsseldorf, Düsseldorf, Germany (T.G.S.), Universitätsklinik für Augenheilkunde, Inselspital, Universität Bern, Bern (M.A.K., K.S., B.E.F.), Institut für Refraktive und Ophthalmo-Chirurgie (IROC), Zürich (T.G.S.), Switzerland, Wellman Center for Photomedicine, Massachusetts General Hospital, Harvard Medical School, Boston, Massachusetts, USA (T.G.S.), and the ARTORG Center for Biomedical Engineering Research, University of Bern, Bern, Switzerland (M.H.N., P.B.).

Inquiries to Dr. Theo G. Seiler, Klinik für Augenheilkunde, Universitätsklinikum Düsseldorf, Moorenstraβe 5, 40225 Düsseldorf, Germany; e-mail: theo@seiler.tv

CORNEAL CROSS-LINKING (CXL) IS AN EFFECTIVE procedure to halt the progression of keratectasia such as keratoconus[1,2] or post–LASIK ectasia[3] with low rates of complication.[4,5] By means of riboflavin as the photosensitizer and the activation by ultraviolet (UV) irradiation, reactive oxygen species (ROS) are created, inducing new bonds in the extracellular matrix of the cornea.[6] If 1 of the 3 "ingredients" does not contribute to the process, CXL is ineffective. The first factor, riboflavin, has been investigated extensively and corneal riboflavin concentrations with an epi-off application have been found to be sufficient,[7] also in deeper corneal layers not restricting CXL. The second, UV light, is not a restricting factor because even at an irradiance of 3 mW/cm^2, CXL demonstrates the best biomechanical effect.[8] Therefore, irradiance cannot be the bottleneck for accelerated epi-off protocols. Richoz and associates[9] performed cross-linking in an oxygen-free environment and found no significant stiffening effect emphasizing the importance of oxygen in CXL. To date, only few reports have been published on the basics of corneal oxygen kinetics during cross-linking[10,11] or on the biomechanical effect of supplementary oxygen during CXL.[10,12]

The aim of this study was to provide experimental data on the oxygen consumption during CXL by determination of the oxygen profile at different depths using different irradiances and oxygen environments. Oxygen kinetics might be the missing piece to understand the invalidity of Bunsen-Roscoe's law in CXL.

MATERIALS AND METHODS

• PREPARATION OF EYES: Freshly enucleated porcine eyes were obtained 2-3 hours postmortem from a local abattoir. The eyes were stored at 4° C and used within 8 hours. Before the experiments, the corneas were examined for corneal opacities and epithelial defects. The eyes were divided into 6 different groups (n = 5 for each group).

0002-9394
https://doi.org/10.1016/j.ajo.2020.11.001

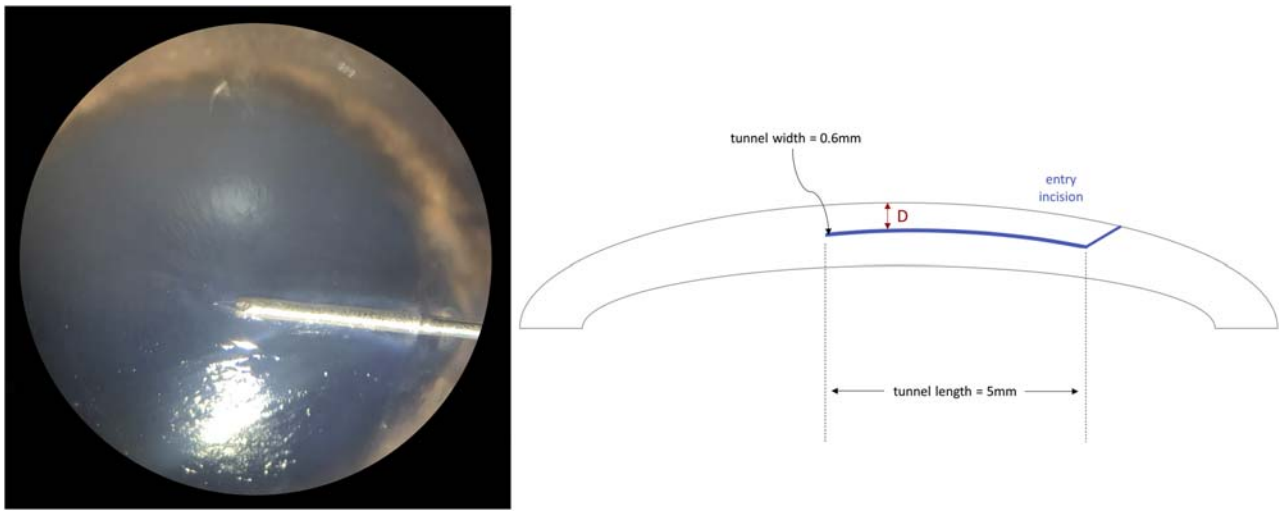

FIGURE 1. Left: Photography with the inserted oxygen sensor inside the stroma at a depth of 200 μm. Right: Schematic illustration of the channel creation. "D" represents the depth of the channel between 100 and 300 μm.

Three of the groups were subjected to CXL in an atmospheric environment (room air, 21% oxygen), whereas the rest of the groups underwent CXL in a hyperoxic environment (>95% oxygen). Before any treatment, the corneal epithelium was removed using a blunt hockey knife, and by means of a femtosecond laser (FEMTO LDV Z8; Ziemer Ophthalmic Systems, Port, Switzerland), a small tunnel with a width of 0.6 mm and length of 5 mm (Figure 1) was created for each subgroup at a depth *D* of either 100, 200, or 300 μm (controlled by optical coherence tomography). The tunnel was generated to guide the oxygen microsensor and to guarantee the proper depth of the sensor within the corneal stroma.

• **OXYGEN MICROSENSOR:** Before data acquisition, the optic oxygen microsensor (NTH-PSt1; PreSens, Regensburg, Germany) was connected to a microfiber optic oxygen meter (Micro TX3; PreSens) and calibrated at room temperature following the manufacturer's guidelines using 2 data points at 0% and 20.9% oxygen. To provide smoother measurements, dynamic signal averaging has been applied, meaning every yielded data point per second consists of an average of 4 measurement points. Because the sensor has a response time of <2 seconds, measurements during the first 2 seconds of each data set were excluded from evaluation. Although the oxygen microsensor has a theoretical limit of detection of 0.05% for gaseous and dissolved O_2, premeasurements in corneal tissue indicated a lower limit of detection of below 1%.[13]

• **OXYGEN MEASUREMENTS AND CROSS-LINKING:** The eyes were kept in a custom-built chamber with 2 access paths for inserting the oxygen microsensor and for applying riboflavin drops and the UV beam. In addition, an oxygen gas tank was connected via a tube to assure an oxygen concentration above 95% for groups with a hyperoxic environment. The oxygen content inside the chamber was controlled during the experiments by a separate oxygen sensor (Fibox 4; PreSens). After mounting the eye, the sensor was inserted into the channel under a microscope, so that the fiberoptic tip of the sensor reached the end of the tunnel to guarantee the proper depth (Figure 1). The oxygen concentration measurements were then initiated, and meanwhile drops of riboflavin 0.1% (VibeX Rapid; Avedro, Waltham, Massachusetts, USA) were applied every 2 minutes for a total of 10 minutes. Then the UV source (KXL; Avedro) was focused onto the surface of the cornea, centered next to the end of the tunnel delivering continuous irradiances ranging from 3 to 30 mW/cm^2 with a diameter of 9 mm. Each measurement was recorded until either an equilibrium of the oxygen concentration had been established or until the concentration decreased to a level of less than 1%.

• **DATA ANALYSIS:** Descriptive statistics were performed using Microsoft Excel. Every experimental data set (1 eye, time course of oxygen concentration in 1 depth during CXL) was fit to reduce the measurement noise (MATLAB R2019b; The MathWorks, Natick, Massachusetts, USA), as presented in Figure 2.

$$O_2 = b_1 e^{b_2 t} + b_3 \quad (1)$$

Where b_1 describes the speed of the oxygen consumption, b_2 represents the negative time constant of the exponential decay, and b_3 is the equilibrium oxygen concentration. To approximate the time constant of the decay, the half-life of each fit function (Eq. 1) was determined, and for the equilibrium oxygen concentration, the fit-parameter b_3 (Eq. 1)

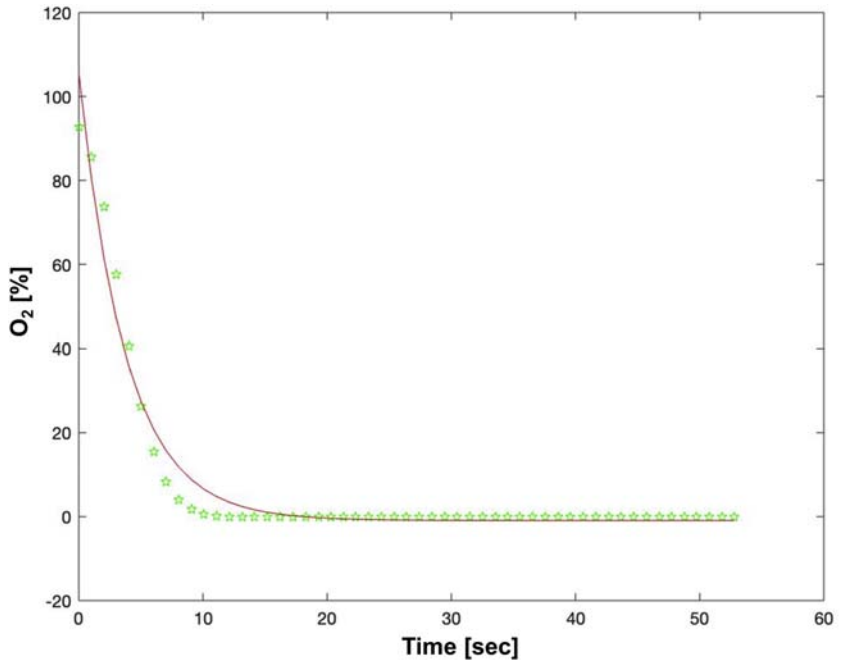

FIGURE 2. Data points at a measurement (green points) and the fit curve (red).

was used. For the initial oxygen depletion rate, the first derivate at t = 1 *second* was taken.

To compare oxygen concentrations between different depths of the cornea, Mann-Whitney *U* tests were performed (Winstat for Excel; R. Finch, Germany). Significance was accepted if $P < .05$.

• **NUMERICAL MODEL:** The transport of oxygen in the cornea is governed by a diffusion equation (Eq. 2):

$$D\frac{\partial^2 P_{O2}}{\partial x^2} - \frac{Q}{k} = \frac{\partial P_{O2}}{\partial t} \tag{2}$$

where D is the diffusivity (mm^2/s), x is the position (mm), P_{O2} is the partial pressure of oxygen ($mmHg$), k is Henry's solubility constant ($mL(O2)/mL(tissue) \times mmHg$), t is time (s), and Q is the oxygen consumption due to the CXL induced by UV light $\left(\frac{mL(O_2)}{mL(tissue) \times s}\right)$. In this study, we assume that this consumption is linearly dependent on the UV irradiance and follows an exponential decay with the distance from the anterior corneal surface. Moreover, a Michaelis-Menten–type relationship for oxygen uptake was used to account for oxygen availability (Eq. 3): where Q_0 $\left(\frac{mL(O_2) \times cm^2}{mL(tissue) \times s \times mW}\right)$ and ζ (μm) are model parameters, W $\left(\frac{mW}{cm^2}\right)$ is the irradiance, and $Q_{stroma}\left(\frac{mL(O_2)}{mL(tissue) \times s}\right)$ is the consumption of oxygen by the stromal cells.[14]

The model was divided into 3 layers: the stroma (0.85 mm), the endothelium (0.005 mm), and a posterior boundary layer (0.1 mm) describing the diffusion kinetic related to the aqueous humor. The diffusivity of the stroma (Dk_{str}) was a model parameter, but the diffusivity of the endothelium and that of the boundary layer were constrained to a fixed ratio ($Dk_{bc} = 0.1\ Dk_{str}$ and $Dk_{end} = 0.2\ Dk_{str}$).[14]

The partial differential equation solver *pdepe* in MATLAB (MATLAB R2019b; The MathWorks) was used to solve the diffusion equation. The different oxygen concentrations were simulated by changing the anterior and posterior boundary conditions; the 100% configuration was modeled with a partial pressure of oxygen of 775 mmHg on the anterior surface and 375 mmHg on the posterior side, whereas the 20% configuration was modeled with pressures of 155 and 50 mmHg on the anterior and posterior side. The values chosen for these boundary conditions were provided by direct measurements of the environmental and aqueous oxygen concentrations. An iterative least-squares

$$Q = Q_{CXL}\frac{P_{O2}}{K + P_{O2}} + Q_{stroma}\frac{P_{O2}(20 + 155)}{155(20 + P_{O2})},\ Q_{CXL} = Q_0 We^{-\chi_\zeta} \tag{3}$$

TABLE 1. Representation of the Equilibrium Oxygen Concentration in Percent (Upper Number) and Half-Lives of the Oxygen Decay in Seconds (Lower Number) for the Different Depths and Irradiations in the Hyperoxic and Normoxic Environment

Hyperoxic	3 mW/cm^2	9 mW/cm^2	18 mW/cm^2	30 mW/cm^2
100 μm	50.2 ± 6.2%	4.8 ± 3.1%	<1.0%	<1.0%
	17.8 ± 6.7 s	8.9 ± 2.7 s	3.2 ± 1.2 s	1.8 ± 1.0 s
200 μm	47.4 ± 6.6%	2.6 ± 3.2%	<1.0%	<1.0%
	15.3 ± 4.1 s	6.9 ± 1.5 s	2.7 ± 0.6 s	1.6 ± 0.5 s
300 μm	39.7 ± 8.1%	1.2 ± 1.8%	<1.0%	<1.0%
	42.9 ± 27.6 s	15.4 ± 8.1 s	6.1 ± 3.2 s	3.9 ± 2.0 s
Normoxic	**3 mW/cm^2**	**9 mW/cm^2**	**18 mW/cm^2**	**30 mW/cm^2**
100 μm	2.3 ± 2.5%	1.0 ± 0.8%	<1.0%	<1.0%
	4.8 ± 1.7 s	2.2 ± 0.9 s	1.8 ± 0.8 s	1.5 ± 0.8 s
200 μm	1.1 ± 0.9%	<1.0%	<1.0%	<1.0%
	7.0 ± 4.0 s	3.0 ± 0.6 s	2.6 ± 0.5 s	2.0 ± 0.6 s
300 μm	<1.0%	<1.0%	<1.0%	<1.0%
	9.2 ± 3.5 s	3.9 ± 0.5 s	3.1 ± 0.3 s	2.9 ± 0.5 s

optimization process was used to determine the 5 model parameters Q_0, Q_{stroma}, ζ, K, and D_{str}, which best reproduced the experimental data for all measurement depths and irradiances.

RESULTS

• **EQUILIBRIUM OXYGEN CONCENTRATION LEVELS FOR DIFFERENT CORNEAL DEPTHS AND IRRADIATIONS:** Once the UV irradiation was initiated, oxygen levels quickly descended and stabilized at an equilibrium. Table 1 shows the equilibrium in percentage of oxygen and the half-life in a hyperoxic environment as well as for an atmospheric oxygen environment, respectively. The highest oxygen availability was found for both groups in the 3 mW/cm^2 subgroup in 100 μm with 2.3 ± 2.5% in the normoxic and 50.2 ± 6.2% in the hyperoxic environment. In both subgroups, decreasing oxygen levels were observed when measured in deeper corneal layers ($P = .009$) or higher irradiances ($P = .009$) illustrated in Figure 3. After cessation of the UV irradiation, oxygen concentrations recovered quickly and returned to initial levels (Figure 4a and b).

• **AVERAGED INITIAL OXYGEN DEPLETION RATES FOR DIFFERENT CORNEAL DEPTHS AND IRRADIATIONS:** Based on the derivative of the corresponding fit function, the initial depletion rate (in combination with the re-diffused oxygen) for the O_2 concentration was calculated. The corresponding depletion rates are listed in Table 2. Depletion rates increase with higher applied irradiances and decrease with depth. An anomaly is observed at 100 μm depth in the hyperoxic subgroup for all irradiances with lower depletion rates than at 200 μm depth.

• **DIFFUSION MODEL:** The experimental decays of the oxygen were fit to Eq. (3). The optimized parameters for all 4 irradiances yielded the following model parameters:

$$Q_0 = 1.45\times 10^{-3}\frac{mL(O_2)\times cm^2}{mL(tissue)\times s\times mW}$$

$$Q_{stroma} = 9.91\times 10^{-6}\ \frac{mL(O_2)}{mL(tissue)\times s}$$

$$\xi = 75.84\ \mu m$$

$$K = 7.57\ mmHg$$

$$Dk_{str} = 4.92\times 10^{-8}\ \frac{mL(O_2)\times mm^2}{mL(tissue)\times mmHg\times s}$$

With these parameters, the model was able to reproduce the measured decay curves mostly within 1 standard deviation. The best fit between the model and the experiment was observed at a depth of 300 μm, whereas the largest difference between the model and the experiments was observed at 100 μm for the different irradiances in the hyperoxic environment (Figure 5).

DISCUSSION

THE MAIN FINDINGS OF THIS STUDY ARE AS FOLLOWS:

(1) Using the conventional 3 mW/cm^2 Dresden protocol, oxygen is available in the anterior 300 μm of the corneal stroma throughout the entire CXL procedure. At irradiances of 9 mW/cm^2 and higher, all

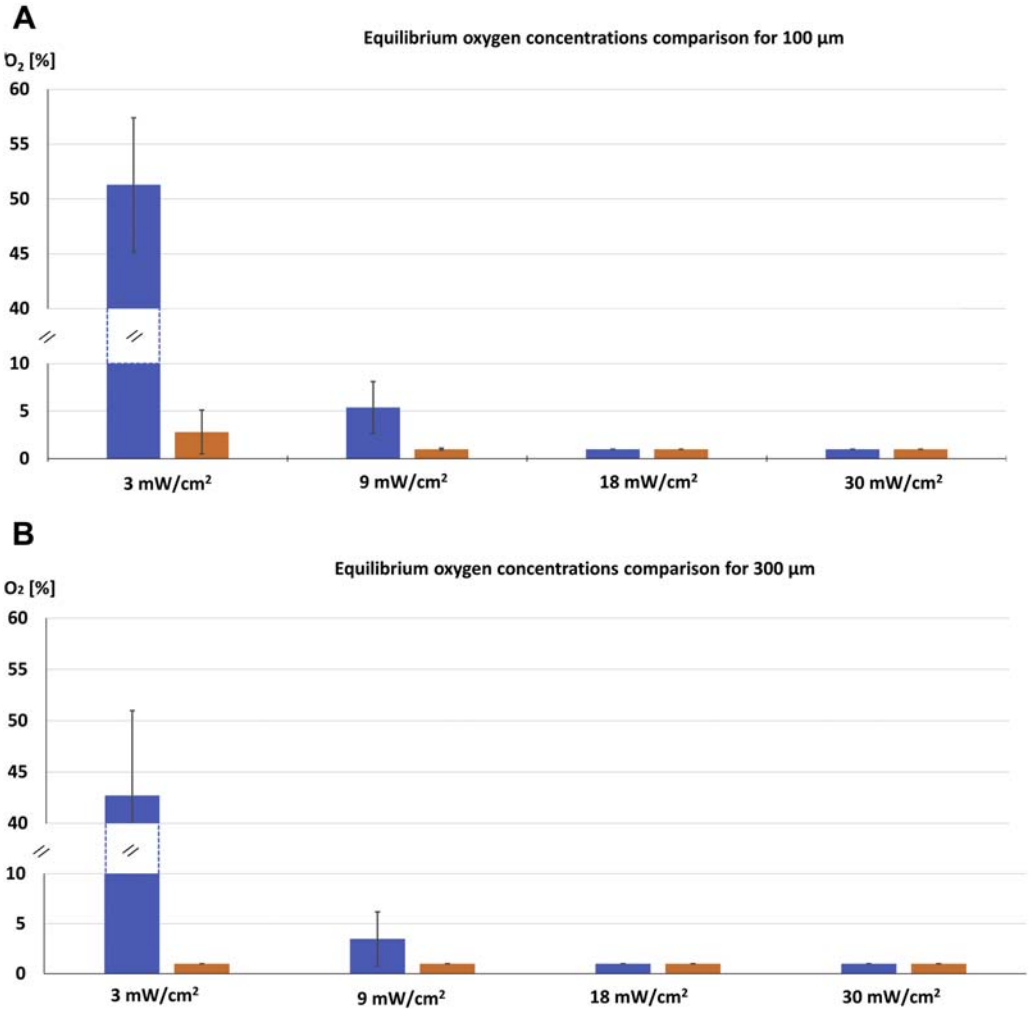

print & web 4C/FPO

FIGURE 3. A. Comparison of equilibrium oxygen concentration ± standard deviation (%) at 100 µm depth. The blue bars represent measurements in a >95% oxygen environment, and the orange bars represent groups from an atmospheric environment. B. Comparison of equilibrium oxygen concentration ± standard deviation (%) at 300 µm depth. The blue bars represent measurements in a >95% oxygen environment, and the orange bars represent groups from an atmospheric environment.

oxygen is consumed within in the anterior 200 µm or 100 µm, respectively.

(2) A hyperoxic environment can substantially increase available stromal oxygen, allowing a sufficient CXL deeper than 300 µm with irradiances less than 18 mW/cm^2.

(3) Higher oxygen depletion rates are found with higher irradiances and at higher oxygen concentrations.

(4) A set of parameters describing the oxygen consumption were identified enabling the calculation of the evolution of the oxygen concentration at any position within the cornea for different UV irradiances.

Besides the well-examined and surplus available factors riboflavin and UV light, a third factor, oxygen, is crucial to achieve sufficient CXL. The mechanism of photosensitized production of ROS such as singlet oxygen has been described before,[15,16] and McCall and associates[17] confirmed this pathway for CXL by ROS inhibitors (azide) or stimulators (D_2O) altering the biomechanical effect of CXL. Kamaev and associates[10] proposed type I (low oxygen availability) and type II (sufficient oxygen availability) reactions and demonstrated experimentally the depletion and thus scarcity of oxygen during CXL. In contrast to our results, they found no residual oxygen later than 15 seconds at 3 mW/cm^2 and 5 seconds at 30 mW/cm^2 irradiation in 100 µm depth. However, they have applied the 0.1% riboflavin in distilled water every 30 seconds for up to 50 minutes leading to massive corneal swelling. With an anticipated flap thickness of >200 µm, their results are in agreement with ours. Recently, also Hill and associates[11] found no oxygen at 200 µm depth using 3 mW/cm^2 in an atmospheric environment, however, with similar

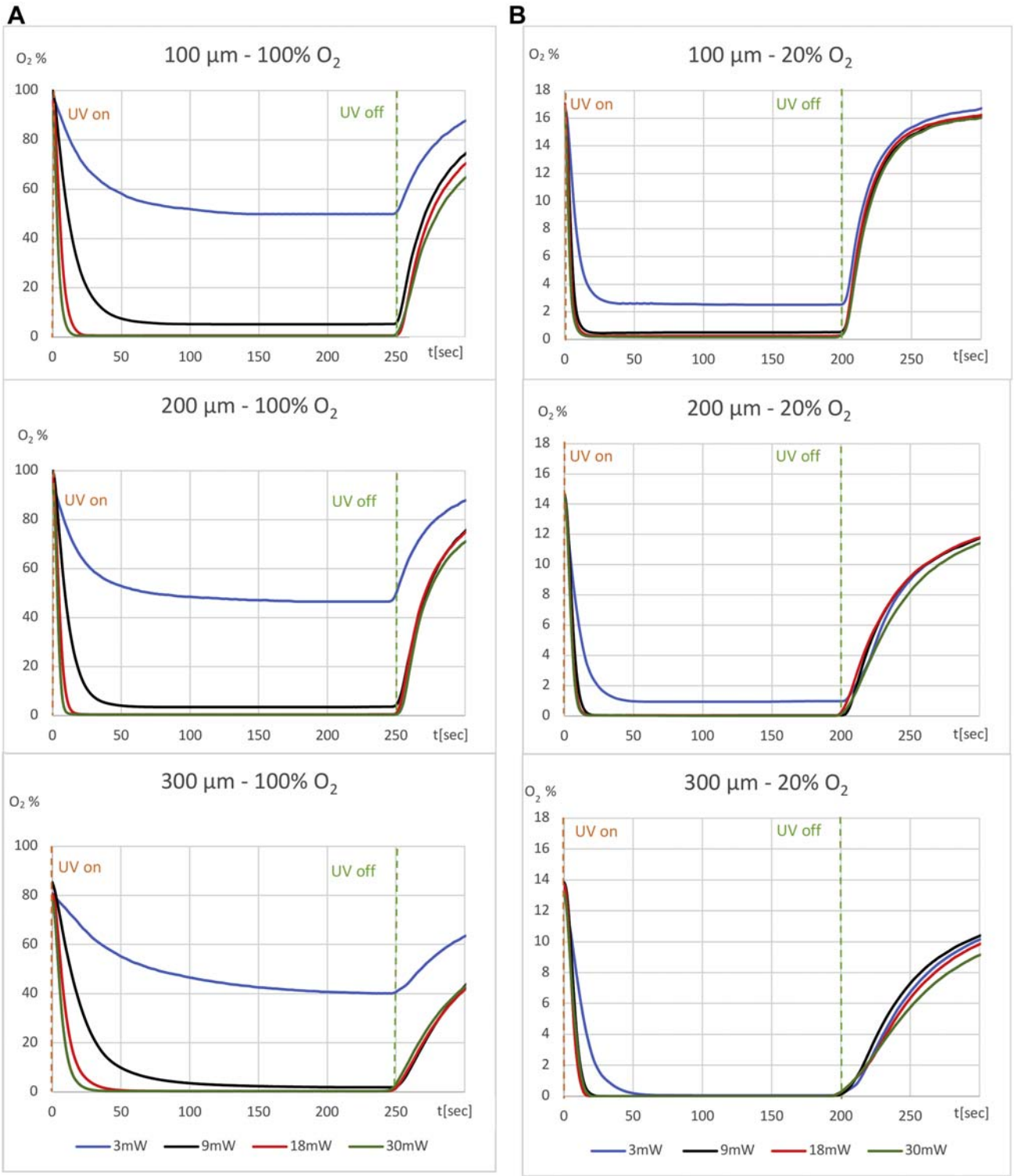

FIGURE 4. A. Averaged oxygen concentrations during the ultraviolet (UV) irradiation at different corneal depths (100, 200, and 300 µm, respectively) for the hyperoxic environment. B. Averaged oxygen concentrations during the UV irradiation at different corneal depths (100, 200, and 300 µm, respectively) for the normoxic environment.

consumption times of around 30 seconds. On the other hand, our finding of stromal oxygen down to 300 µm at 3 mW/cm^2 and down to 200 µm at 9 mW/cm^2 at atmospheric oxygen conditions matches clinically determined demarcation line depth.[18] To date there are no further publications reporting oxygen levels and consumption times

TABLE 2. Average Absolute Values of Depletion Rates and Standard Deviations in % Oxygen/Second for the Hyperoxic and Normoxic Environment in Different Irradiations and Depths

Hyperoxic	3 mW/cm^2	9 mW/cm^2	18 mW/cm^2	30 mW/cm^2
100 μm	1.9 ± 0.4 %O_2/s	8.1 ± 1.6 %O_2/s	27.7 ± 9.8 %O_2/s	49.7 ± 15.0 %O_2/s
200 μm	2.2 ± 0.8 %O_2/s	11.1 ± 3.5 %O_2/s	31.9 ± 9.3 %O_2/s	57.3 ± 19.2 %O_2/s
300 μm	0.9 ± 0.5 %O_2/s	5.3 ± 2.8 %O_2/s	14.5 ± 8.3%O_2/s	21.7 ± 14.8 %O_2/s
Normoxic	3 mW/cm^2	9 mW/cm^2	18 mW/cm^2	30 mW/cm^2
100 μm	2.6 ± 0.8 %O_2/s	7.3 ± 2.4 %O_2/s	10.2 ± 3.9 %O_2/s	10.8 ± 12.2 %O_2/s
200 μm	1.9 ± 1.0 %O_2/s	4.4 ± 1.2 %O_2/s	5.5 ± 1.4 %O_2/s	6.7 ± 1.6 %O_2/s
300 μm	1.1 ± 0.6 %O_2/s	2.2 ± 0.45 %O_2/s	2.5 ± 0.4 %O_2/s	2.5 ± 0.2 %O_2/s

for epi-off CXL at atmospheric oxygen levels. Based on our data for atmospheric oxygen conditions, the maximum CXL effect has to be expected at 3 mW/cm^2 and less, which is also supported by theoretical and experimental data.[8,19] For hyperoxic conditions, the optimal irradiance lays somewhere between 9 and 18 mW/cm^2 because the oxygen concentration is above 1% until a depth of 300 μm and deeper for 9 mW/cm.[2] It is obvious that with a continuous irradiance of 30 mW/cm^2 even a hyperoxic atmosphere over the cornea does not provide enough oxygen, not even at the 100 μm level (Table 1).

Diakonis and associates[12] investigated experimentally the biomechanical effect of epi-off CXL at a hyperoxic environment using a continuous 30 mW/cm^2 irradiation and reported no significant effect. This is in accordance with the data presented here, because the biomechanical testing was performed in 100 μm and deeper, for which our data show no sufficient diffusion of oxygen for either atmospheric or hyperoxic conditions. In addition, the oxygen gas stream was directed onto the cornea without establishing a controlled enriched oxygen environment. Hill and associates[11] investigated the benefit of supplementary oxygen only for transepithelial CXL. A comparison is almost impossible because the riboflavin imbibition solution had a 2.5-fold higher riboflavin concentration than for epi-off, leading to a totally different stromal riboflavin gradient and UV-absorption characteristics and, therefore, incomparable oxygen dynamics. In addition, it is well known that the epithelium alone consumes nearly as much oxygen as stroma and endothelium together.[20,21] Weng and associates[22] investigated the use of oxygen enrichment at 3 mW/cm^2 with only insignificant superiority of the group with supplementary oxygen. This is in accordance with the data presented here, because at 3 mW/cm^2 a surplus of oxygen exists until a depth of 300 μm even under atmospheric oxygen conditions.

We found higher oxygen depletion rates with increasing irradiances and oxygen concentrations. This can somewhat be expected, because higher energy input causes higher consumption of available factors. In addition, the numerical model indicates that there is a strong depth dependence of the oxygen depletion, following an exponential decay. This spatial decay agrees with the theoretical model proposed by Kling and Hafezi[23] to quantify the mechanical stiffening of CXL. However, to the best of our knowledge, no numerical model was calibrated on direct measurements of the oxygen concentration at different depths within the cornea during the CXL process. This information provides the basis for a precise quantification of the spatial distribution of oxygen depletion by CXL, which serves as a basis of models accounting for the photochemical kinetics of CXL.[11,23]

One of the challenges of the numerical modeling concerns the boundary condition on the posterior surface of the cornea. Because of the ex vivo nature of the experiments, the oxygen concentration in the aqueous humor is not regulated and is only affected by the environmental oxygen concentration (normoxic vs hyperoxic). However, this diffusion process is also changing when the UV irradiation depletes the corneal oxygen. The effect has been observed experimentally by direct measurement of the aqueous oxygen. To account for this effect, our model includes an additional boundary layer on the posterior side of the cornea to allow for the oxygen to diffuse from the aqueous humor. However, the oxygen diffusivity identified in this study is in the range of values previously published for human and rabbit corneas, which indicates that both the experimental measurements and numerical model produce pertinent data.[14,24]

Another interesting issue arises from longer half-lives and lower depletion rates at a depth of 200 μm compared with 100 μm in a hyperoxic environment. Shorter times and higher depletion rates due to a higher UV intensity[25] and more riboflavin[7] would be expected for 100 μm depth compared with 200 μm, similar to what we found in the atmospheric group. A suspected reason for these systematically longer half-lives and lower depletion rates at 100 μm may be the substantially higher oxygen diffusion from the surface into the anterior stroma under hyperoxic conditions.

From the point of view of clinical implication, our findings suggest that supplementary oxygen might increase the aerobic type II reaction enabling a potentially deeper and more effective CXL. This seems to be valid for all examined

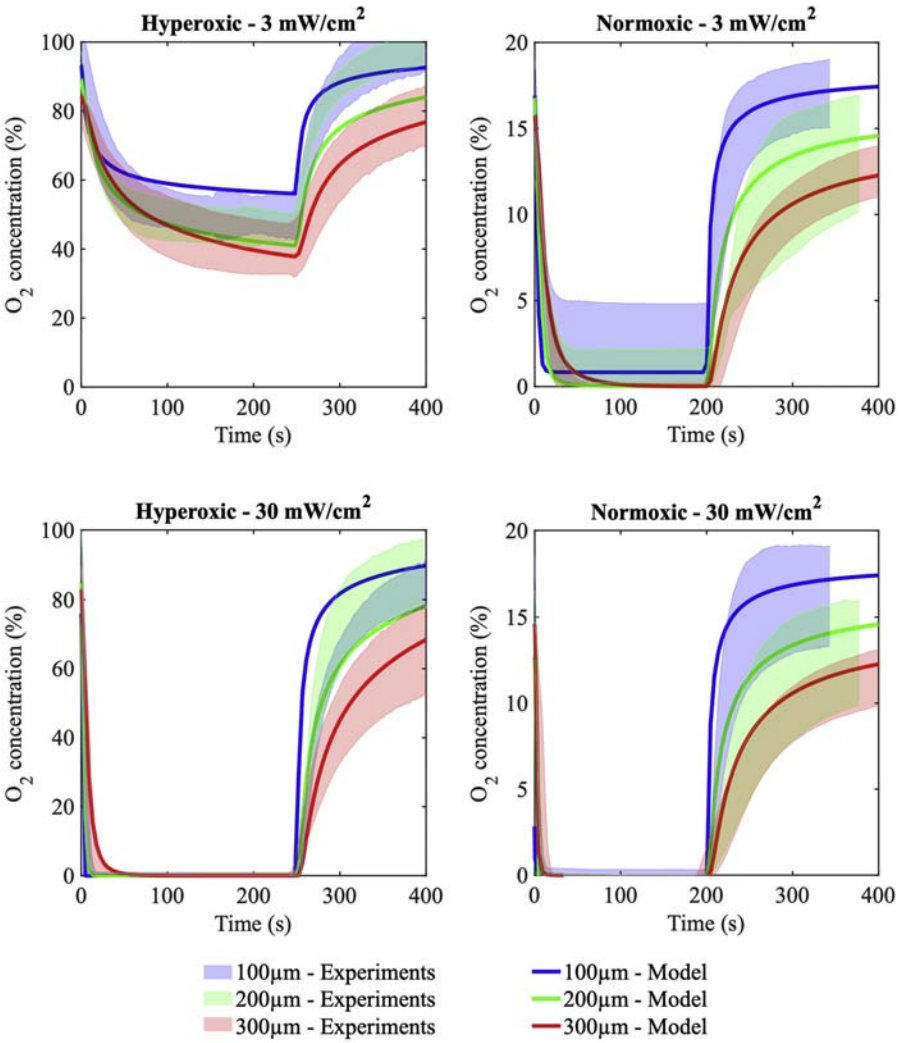

FIGURE 5. The oxygen concentration calculated after identification of the parameters (solid lines) was compared with the experimental data (shaded area) for the different environments (hyperoxic and normoxic), and CXL irradiances (3 and 30 mW/cm^2) and depths (100, 200, and 300 µm). The shade area represents ±1 standard deviation around the average experimental curve.

irradiances; however, as mentioned above, the optimum continuous UV irradiance for epi-off CXL with supplementary oxygen must be assumed between 9 and 18 mW/cm^2. For CXL at atmospheric oxygen conditions, the low oxygen availability can explain the better experimental outcome[8] for lower irradiances. On the other hand, similar clinical results have been observed after CXL for irradiances[26] between 3 and 30 mW/cm^2. It is known that all protocols achieve a CXL effect, although less and limited to the superficial corneal layers with higher irradiances. The only morphologic difference, however, is the depth of the demarcation line.[27,28] It is remarkable that lower irradiances produce deeper demarcation lines showing a good correlation with the oxygen kinetics found in this study. However, it is still unknown how much CXL is required to stabilize keratoconus.

Finally, the observation of lower oxygen availability at higher irradiances can explain the invalidity of the Bunsen-Roscoe law for CXL. Shorter irradiation times with similar radiant exposures result in less time for oxygen re-diffusion and, therefore, lower total oxygen availability for CXL. However, experimental biomechanical measurements are required to proof this hypothesis.

A limitation of the study is the use of ex vivo porcine eyes, which may not account for physiological consumption inside the cornea as well as for diffusion of oxygen from and into the aqueous humor. In addition, paired eyes would have allowed a better comparison between the normoxic and hyperoxic environment; however, because of logistical reasons at the abattoir, this was not possible. Also, the sensitivity of the oxygen microsensor below 1% in corneal tissue limits conclusions for subtle

differences for higher irradiances. The concern of potential oxygen leakage through the tunnel can be ruled out, because the re-diffusion times for the various depths differ substantially (Figure 4).

In conclusion, the results presented here provide new information on the oxygen kinetics during riboflavin-mediated CXL and can explain experimental and clinical findings on the effect of CXL with higher irradiances.

ALL AUTHORS HAVE COMPLETED AND SUBMITTED THE ICMJE FORM FOR DISCLOSURE OF POTENTIAL CONFLICTS OF INTEREST. Funding/Support: M.H.N. was supported by the Swiss National Science Foundation, Switzerland with the project IZLIZ3_182975. Financial Disclosures: None of the authors has any financial interests. All authors attest that they meet the current ICMJE criteria for authorship.

Acknowledgments: The authors thank Professor Irene Kochevar, PhD, for the inspiring discussion and support. They also thank Avedro Inc and Glaukos Corp (Waltham, Massachusetts, USA) for the material support with VibeX Rapid and the allocation of the KXL UV source, and Ziemer Ophthalmic Systems (Port, Switzerland) for their support with the channel creation using the Z8.

REFERENCES

1. Wollensak G, Spoerl E, Seiler T. Riboflavin/ultraviolet-a-induced collagen crosslinking for the treatment of keratoconus. *Am J Ophthalmol* 2003;135:620–627.
2. Raiskup F, Theuring A, Pillunat LE, Spoerl E. Corneal collagen crosslinking with riboflavin and ultraviolet-A light in progressive keratoconus: ten-year results. *J Cataract Refract Surg* 2015;41:41–46.
3. Hafezi F, Kanellopoulos J, Wiltfang R, Seiler T. Corneal collagen crosslinking with riboflavin and ultraviolet A to treat induced keratectasia after laser in situ keratomileusis. *J Cataract Refract Surg* 2007;33:2035–2040.
4. Seiler TG, Schmidinger G, Fischinger I, Koller T, Seiler T. Complications of corneal cross-linking. *Ophthalmologe* 2013;110:639–644 [in German].
5. Hersh PS, Stulting RD, Muller D, Durrie DS, Rajpal RK. United States multicenter clinical trial of corneal collagen crosslinking for keratoconus treatment. *Ophthalmology* 2017;124:1259–1270.
6. Hayes S, Kamma-Lorger CS, Boote C, et al. The effect of riboflavin/UVA collagen cross-linking therapy on the structure and hydrodynamic behaviour of the ungulate and rabbit corneal stroma. *PLoS One* 2013;8:e52860.
7. Ehmke T, Seiler TG, Fischinger I, Ripken T, Heisterkamp A, Frueh BE. Comparison of corneal riboflavin gradients using dextran and HPMC solutions. *J Refract Surg* 2016;32:798–802.
8. Hammer A, Richoz O, Arba Mosquera S, Tabibian D, Hoogewoud F, Hafezi F. Corneal biomechanical properties at different corneal cross-linking (CXL) irradiances. *Invest Ophthalmol Vis Sci* 2014;55:2881–2884.
9. Richoz O, Hammer A, Tabibian D, Gatzioufas Z, Hafezi F. The biomechanical effect of corneal collagen cross-linking (CXL) with riboflavin and UV-A is oxygen dependent. *Transl Vis Sci Technol* 2013;2:6.
10. Kamaev P, Friedman MD, Sherr E, Muller D. Photochemical kinetics of corneal cross-linking with riboflavin. *Invest Ophthalmol Vis Sci* 2012;53:2360–2367.
11. Hill J, Liu C, Deardorff P, et al. Optimization of oxygen dynamics, UV-A delivery, and drug formulation for accelerated epi-on corneal crosslinking. *Curr Eye Res* 2020;45:450–458.
12. Diakonis VF, Likht NY, Yesilirmak N, et al. Corneal elasticity after oxygen enriched high intensity corneal cross linking assessed using atomic force microscopy. *Exp Eye Res* 2016;153:51–55.
13. PreSens. Needle-type oxygen microsensor NTH-PSt1. Available at https://www.presens.de/products/detail/needle-type-oxygen-microsensor-nth-pst1. Accessed May 2, 2020.
14. Larrea X, Büchler P. A transient diffusion model of the cornea for the assessment of oxygen diffusivity and consumption. *Invest Ophthalmol Vis Sci* 2009;50:1076–1080.
15. Shimizu R, Yagi M, Kikuchi A. Suppression of riboflavin-sensitized singlet oxygen generation by l-ascorbic acid, 3-O-ethyl-l-ascorbic acid and Trolox. *J Photochem Photobiol B* 2019;191:116–122.
16. Kochevar IE, Redmond RW. Photosensitized production of singlet oxygen. *Methods Enzymol* 2000;319:20–28.
17. McCall AS, Kraft S, Edelhauser HF, et al. Mechanisms of corneal tissue cross-linking in response to treatment with topical riboflavin and long-wavelength ultraviolet radiation (UVA). *Invest Ophthalmol Vis Sci* 2010;51:129–138.
18. Brittingham S, Tappeiner C, Frueh BE. Corneal cross-linking in keratoconus using the standard and rapid treatment protocol: differences in demarcation line and 12-month outcomes. *Invest Ophthalmol Vis Sci* 2014;55:8371–8376.
19. Kling S, Hafezi F. Biomechanical stiffening: slow low-irradiance corneal crosslinking versus the standard Dresden protocol. *J Cataract Refract Surg* 2017;43:975–979.
20. Freeman RD. Oxygen consumption by the component layers of the cornea. *J Physiol* 1972;225:15–32.
21. Harvitt DM, Bonanno JA. Oxygen consumption of the rabbit cornea. *Invest Ophthalmol Vis Sci* 1998;39:444–448.
22. Wang J, Wang L, Li Z, Wang YM, Zhu K, Mu G. Corneal biomechanical evaluation after conventional corneal crosslinking with oxygen enrichment. *Eye Contact Lens* 2020;46:306–309.
23. Kling S, Hafezi F. An algorithm to predict the biomechanical stiffening effect in corneal cross-linking. *J Refract Surg* 2017;33:128–136.
24. Fatt I, Freeman RD, Lin D. Oxygen tension distributions in the cornea: a re-examination. *Exp Eye Res* 1974;18:357–365.
25. Spoerl E, Mrochen M, Sliney D, Trokel S, Seiler T. Safety of UVA-riboflavin cross-linking of the cornea. *Cornea* 2007;26:385–389.
26. Shajari M, Kolb CM, Agha B, et al. Comparison of standard and accelerated corneal cross-linking for the treatment of keratoconus: a meta-analysis. *Acta Ophthalmol* 2019;97:e22–e35.
27. Asgari S, Hashemi H, Hajizadeh F, et al. Multipoint assessment of demarcation line depth after standard and accelerated cross-linking in central and inferior keratoconus. *J Curr Ophthalmol* 2018;30:223–227.
28. Mazzotta C, Hafezi F, Kymionis G, et al. In vivo confocal microscopy after corneal collagen crosslinking. *Ocul Surf* 2015;13:298–314.